Journal of Applied Physics

Electronic structure evolution in dilute carbide $Ge_{1-x}C_x$ alloys and implications for device applications

Cite as: J. Appl. Phys. **126**, 195702 (2019); https://doi.org/10.1063/1.5111976
Submitted: 03 June 2019 . Accepted: 09 September 2019 . Published Online: 20 November 2019

Christopher A. Broderick, Michael D. Dunne, Daniel S. P. Tanner, and Eoin P. O'Reilly

Journal of Applied Physics ARTICLE scitation.org/journal/jap

Electronic structure evolution in dilute carbide $Ge_{1-x}C_x$ alloys and implications for device applications

Cite as: J. Appl. Phys. **126**, 195702 (2019); doi: 10.1063/1.5111976
Submitted: 3 June 2019 · Accepted: 9 September 2019 ·
Published Online: 20 November 2019

Christopher A. Broderick,[1,2,a)] Michael D. Dunne,[1,2] Daniel S. P. Tanner,[1] and Eoin P. O'Reilly[1,2]

AFFILIATIONS

[1]Tyndall National Institute, University College Cork, Lee Maltings, Dyke Parade, Cork T12 R5CP, Ireland
[2]Department of Physics, University College Cork, Cork T12 YN60, Ireland

Note: This paper is part of the Special Topic on Highly Mismatched Semiconductors Alloys: from Atoms to Devices.
[a)]**Electronic mail:** c.broderick@umail.ucc.ie

ABSTRACT

We present a theoretical analysis of electronic structure evolution in the highly-mismatched dilute carbide group-IV alloy $Ge_{1-x}C_x$. For ordered alloy supercells, we demonstrate that C incorporation strongly perturbs the conduction band (CB) structure by driving the hybridization of A_1-symmetric linear combinations of Ge states lying close in energy to the CB edge. This leads, in the ultradilute limit, to the alloy CB edge being formed primarily of an A_1-symmetric linear combination of the L-point CB edge states of the Ge host matrix semiconductor. Our calculations describe the emergence of a "quasidirect" alloy bandgap, which retains a significant admixture of indirect Ge L-point CB edge character. We then analyze the evolution of the electronic structure of realistic (large, disordered) $Ge_{1-x}C_x$ alloy supercells for C compositions up to $x = 2\%$. We show that short-range alloy disorder introduces a distribution of localized states at energies below the Ge CB edge, with these states acquiring minimal direct (Γ) character. Our calculations demonstrate strong intrinsic inhomogeneous energy broadening of the CB edge Bloch character, driven by hybridization between Ge host matrix and C-related localized states. The trends identified by our calculations are markedly different to those expected based on a recently proposed interpretation of the CB structure based on the band anticrossing model. The implications of our findings for device applications are discussed.

I. INTRODUCTION

The indirect fundamental bandgaps of the group-IV semiconductors silicon (Si) and germanium (Ge) lead to intrinsically inefficient emission and absorption of light, rendering these materials unsuitable for applications in (active) photonic or photovoltaic devices. At present, the development of Si photonics is limited by a lack of direct-gap materials which are both suitable for applications in semiconductor lasers and light-emitting diodes and compatible with established complementary metal-oxide semiconductor (CMOS) fabrication and processing infrastructure.[1–3] Similarly, direct-gap semiconductors having a fundamental bandgap of ≈1 eV and lattice constants commensurate with growth on Ge are required to facilitate the development of highly efficient multijunction solar cells.[4–6] To overcome this challenge, there has been a strong surge of interest in engineering the band structure of group-IV materials—in particular, Ge, via strain or alloying—to produce semiconductors possessing a direct fundamental bandgap.[7,8] To date, these efforts have centered on the application of tensile strain to Ge[9–12] and on tin- (Sn-) containing $Ge_{1-x}Sn_x$ alloys.[13–18] Given the opportunities and challenges associated with direct-gap group-IV semiconductors, broader interest in related group-IV alloys containing lead[19–23] (Pb) and carbon[24–27] (C) has begun to develop.

Initial interest in dilute carbide group-IV alloys originated over two decades ago, as a means to ameliorate issues related to the high levels of strain in Si_xGe_{1-x}/Ge heterostructures.[28–30] Related theoretical analyses have focused on the impact of C incorporation on the structural, vibrational, and transport properties of ternary dilute $Si_yGe_{1-x-y}C_x$ alloys.[31,32] To date, there have been few theoretical investigations of the implications of dilute C incorporation on the electronic structure of group-IV materials. The recent establishment of novel epitaxial techniques to enable substitutional incorporation of C in Ge opens up the potential to develop

electronic, photonic, and photovoltaic devices based on dilute carbide $Ge_{1-x}C_x$ alloys.[24] However, previous investigations of $Ge_{1-x}C_x$ alloys have provided a range of qualitatively conflicting conclusions, including observations of strong bandgap bowing,[33] a linear increase in bandgap with increasing C composition x,[34] or the emergence of a direct bandgap for a limited range of C compositions.[35]

Several studies have highlighted the challenges associated with the growth of high quality substitutional $Ge_{1-x}C_x$ alloys: because C–C bonds are stronger than Ge–C bonds, there is a strong tendency during growth to form C-related defect clusters.[36] Consistent with this analysis, Park *et al.*[37] showed that it would be virtually impossible to achieve fully substitutional growth of $Ge_{1-x}C_x$ alloys by conventional molecular beam epitaxy (MBE) techniques. Recently, Stephenson *et al.*[38] presented a route to overcome this problem, using a hybrid gas/solid-source MBE approach with tetrakis(germyl)methane (4GeMe) as the C source, a molecule that has one C atom bonded to four Ge atoms. This enabled the growth of high quality $Ge_{1-x}C_x$ alloys having C compositions $x \approx 0.2\%$ C.[24] These samples have been characterized using structural techniques and photomodulated reflectance spectroscopy,[24] but there has been no reports of optical emission to date. Given the limited availability of experimental and theoretical data for $Ge_{1-x}C_x$ alloys, there is little information available in the literature regarding the alloy electronic structure. Recently, two theoretical analyses based on density functional theory (DFT) calculations have provided significant new insight into the $Ge_{1-x}C_x$ electronic structure. Stephenson *et al.*[25] used hybrid functional DFT to compute the band structure of ordered $Ge_{N-1}C_1$ ($x = \frac{1}{N}$) alloy supercells containing $N \leq 128$ atoms ($x \geq 0.78\%$) and demonstrated that C incorporation strongly perturbs the conduction band (CB) structure. On the basis of these calculations, the authors of Ref. 25 suggested that substitutional C acts as an isovalent impurity in Ge, giving rise to a C-related localized impurity state lying ≈0.4 eV above the Ge CB minimum. It was further suggested that this C-related localized impurity state undergoes a band anticrossing (BAC) interaction with the extended zone-center Γ_{7c} CB edge states of the Ge host matrix semiconductor—similar to that in the III-V dilute nitride alloy GaN_xAs_{1-x}[39–42]—resulting in (i) strong reduction of the fundamental bandgap, (ii) the formation of a direct bandgap for $x \gtrsim 0.8\%$, and (iii) closing of the alloy bandgap for $x \lesssim 1.8\%$. However, suggestions regarding the presence and impact of a BAC interaction involving C-related localized states were drawn based on qualitative inspection of the calculated supercell band structures, without quantitative supporting analysis.

More recently, Kirwan *et al.*[27] also presented hybrid functional DFT calculations for ordered $Ge_{1-x}C_x$ alloy supercells. Here, supercell band structure calculations were supported by quantitative analysis of the character of the alloy CB edge states, as encapsulated in the bandgap pressure coefficients. The calculated alloy bandgap pressure coefficient was found to remain, independently of C composition x, approximately equal to that of the indirect (fundamental) L_{6c}-Γ_{8v} bandgap of the Ge host matrix, suggesting limited hybridization of the CB edge with Ge Γ_{7c} states. These calculations indicate the presence of a C-related localized state lying energetically within the bandgap of the Ge host matrix, close in energy to the Ge CB minimum. However, analysis of the calculated alloy bandgap pressure coefficients produced results inconsistent with the presence of a BAC interaction in $Ge_{1-x}C_x$, indicating instead that (i) C incorporation primarily drives hybridization between the Γ_{7c} and X_{5c} CB edge states of Ge, and (ii) the alloy CB edge retains primarily indirect Ge L_{6c} character.

Given these conflicting reports, further theoretical insight is required to quantify the nature and evolution of the $Ge_{1-x}C_x$ electronic structure so that the potential of the alloy for practical applications can be assessed. In this paper, we calculate the electronic structure of idealized (ordered) $Ge_{N-1}C_1$ alloy supercells and of realistic (large, disordered) $Ge_{1728-M}C_M$ ($x = \frac{M}{1728}$) alloy supercells containing a statistically random distribution of M substitutional C atoms. While previous DFT-based analyses have been limited to ordered supercells containing ≤ 128 atoms ($x \geq 0.78\%$), we adopt a semiempirical theoretical framework that allows high-throughput calculations to be performed for large supercells containing $\gtrsim 10^3$ atoms. Using this approach, we quantify (i) the impact of C incorporation on the Ge electronic structure in the ultradilute (impurity) limit, (ii) the impact of short-range alloy disorder (including C clustering) on the electronic structure, and (iii) the evolution of the electronic structure with C composition x in large, disordered alloy supercells.

We explicitly demonstrate the presence of C-induced hybridization of Ge host matrix CB edge states in ordered alloy supercells and demonstrate that the $Ge_{1-x}C_x$ alloy CB edge retains primarily indirect (Ge L_{6c}) character. Explicit analysis of the CB eigenstates in supercells containing up to 2000 atoms provides a broader picture of the electronic structure evolution. Specifically, we confirm that $Ge_{1-x}C_x$ admits a "quasidirect" bandgap in ordered alloy supercells: while the CB minimum appears at the zone center of a $Ge_{N-1}C_1$ supercell, the associated eigenstate in selected supercells is formed predominantly of a linear combination of Ge L_{6c} CB edge states having purely *s*-like orbital character at the C lattice site. We further demonstrate that the alloy CB edge exhibits minimal localization with increasing supercell size, challenging the suggestion that the introduction of an isolated substitutional C atom in Ge generates a (strongly) localized impurity state. For disordered alloy supercells, we find that short-range alloy disorder gives rise to a distribution of C-related localized states—associated with nearest-neighbor C–C pairs, as well as larger clusters of substitutional C atoms and various C-Ge-C type neighbor complexes—lying energetically within the Ge bandgap, with these states acquiring minimal direct (Ge Γ_{7c}) character. Overall, our analysis reveals behavior that is markedly different to that expected on the basis of the BAC model and, in agreement with the conclusions of Kirwan *et al.*,[27] we demonstrate that C incorporation does not drive the formation of a direct bandgap.

The remainder of this paper is organized as follows. In Sec. II, we describe the semiempirical framework we have established to calculate the structural and electronic properties of $Ge_{1-x}C_x$ alloys. The results of our calculations are presented in Sec. III, beginning in Sec. III A with an analysis of the impact of C incorporation on the band structure of small ordered $Ge_{1-x}C_x$ alloy supercells. This is followed by a respective analysis of the character—in Sec. III B—and localization—in Sec. III C—of the CB states as a function of x in ordered supercells containing up to $N = 2000$ atoms. In Sec. III D, we analyze the electronic structure evolution in large, disordered $Ge_{1-x}C_x$ alloy supercells. In Sec. IV, the implications of our results

for device applications are briefly described. Finally, in Sec. V, we summarize and conclude.

II. THEORETICAL MODEL

Highly-mismatched semiconductor alloys are characterized by constituent elements differing significantly in size (covalent radius) and chemical properties (valence orbital energies), resulting in (i) significant changes to the electronic structure of the host matrix semiconductor in response to incorporation of dilute concentrations of the alloying element and (ii) strong sensitivity of the electronic structure to short-range alloy disorder.[40–42] From a technical perspective, these factors constitute a breakdown of the virtual crystal approximation (VCA), mandating direct atomistic calculations in order to capture—even qualitatively—the evolution of the alloy electronic structure.

Beginning with an N-atom Ge_N supercell, the smallest C composition that can be treated is $x = \frac{1}{N}$ in an ordered $Ge_{N-1}C_1$ alloy supercell. Investigation of the material properties in the dilute composition (impurity) limit is therefore limited by the maximum supercell size that can be treated by the electronic structure method employed, and the use of ordered supercells to achieve dilute compositions precludes the investigation of alloy disorder effects. First principles methods that accurately describe the electronic properties of semiconductors are in practice limited to supercells containing $N \lesssim 10^2$ atoms, allowing access to compositions $\sim$1% but providing limited scope to investigate isolated impurities or to quantify alloy disorder effects.

Our theoretical analysis of dilute $Ge_{1-x}C_x$ alloys is therefore based on a semiempirical framework, which can be extended to large system sizes to enable quantitative atomistic analysis of the impact of alloy disorder and related effects in realistic ($N \gtrsim 10^3$, disordered) alloy supercells. First, we use a parameterized valence force field (VFF) potential to perform structural relaxation of alloy supercells.[43] Second, the electronic structure of relaxed alloy supercells is computed using a nearest-neighbor sp^3s^* tight-binding (TB) Hamiltonian.[26] Both the VFF potential and TB Hamiltonian are parameterized via the bulk structural, elastic, and electronic properties of the constituent materials—i.e., the elemental and compound materials formed by nearest-neighbor bonds in a given alloy supercell—which for $Ge_{1-x}C_x$ are the elemental diamond-structured group-IV semiconductors Ge and C, and the zinc blende IV-IV compound GeC (zb-GeC).[44,45]

A. Valence force field potential

We use the modified form[46] of the VFF potential introduced by Musgrave and Pople,[47] whereby the contribution to the lattice free energy associated with an atom located at lattice site i is

$$V_i = \frac{1}{2}\sum_j \frac{k_r}{2}\left(r_{ij} - r_{ij}^{(0)}\right)^2 + \sum_j \sum_{k>j} \left[\frac{k_\theta}{2} r_{ij}^{(0)} r_{ik}^{(0)} \left(\theta_{ijk} - \theta_{ijk}^{(0)}\right)^2 + k_{rr}\left(r_{ij} - r_{ij}^{(0)}\right)\left(r_{ik} - r_{ik}^{(0)}\right) + k_{r\theta}\left(r_{ij}^{(0)}\left(r_{ij} - r_{ij}^{(0)}\right) + r_{ik}^{(0)}\left(r_{ik} - r_{ik}^{(0)}\right)\right)\left(\theta_{ijk} - \theta_{ijk}^{(0)}\right)\right], \quad (1)$$

TABLE I. Equilibrium bond lengths $r^{(0)}$, and force constants k_r, k_θ, k_{rr}, and $k_{r\theta}$, used to implement structural relaxations for $Ge_{1-x}C_x$ alloy supercells using the VFF potential of Eq. (1). Force constants have been computed analytically based on DFT-calculated structural properties for Ge, C, and zb-GeC.[43,44]

Parameter	Unit	Ge	C	zb-GeC
$r^{(0)}$	Å	2.445	1.530	1.969
k_r	eV Å^{-2}	7.0414	26.4077	11.8086
k_θ	eV Å^{-2} rad^{-2}	0.5104	3.7208	1.0780
k_{rr}	eV Å^{-2}	0.2416	0.9740	1.0557
$k_{r\theta}$	eV Å^{-2} rad^{-1}	0.3005	1.7832	1.2515

where j and k index the nearest-neighbor atoms of atom i, $r_{ij}^{(0)}$ and r_{ij}, respectively, denote the unstrained (equilibrium) and relaxed bond lengths between atoms i and j, and $\theta_{ijk}^{(0)}$ and θ_{ijk}, respectively, denote the unstrained and relaxed angles formed by adjacent nearest-neighbor bonds, between atoms i and j, and between atoms i and k. The first and second terms in Eq. (1), respectively, describe contributions to the lattice free energy associated with pure bond stretching and pure bond-angle bending, while the third and fourth terms are "cross terms" which, respectively, describe the impact of changes in r_{ik} on r_{ij}, and the impact of changes in θ_{ijk} on both r_{ij} and r_{ik}.

Recasting Eq. (1) in terms of macroscopic and internal strains allows the force constants k_r, k_θ, k_{rr}, and $k_{r\theta}$ to be determined analytically in terms of the elastic constants C_{11}, C_{12}, and C_{44}, and the Kleinman (internal strain) parameter ζ for diamond or weakly-polar zinc blende structured materials.[43,48] This provides an exact description of the static lattice properties in the linear elastic limit, circumventing the conventional requirement to determine the VFF force constants via numerical fitting. The unstrained bond lengths and VFF force constants used in our calculations are provided in Table I. Full details of the parameterization (via hybrid functional DFT calculations) and benchmarking (vs hybrid functional DFT alloy supercell relaxations) of Eq. (1) for $Ge_{1-x}C_x$ and related group-IV alloys will be presented in Ref. 44. Structural relaxations—implemented using the General Utility Lattice Program (GULP)[49–51]—for $Ge_{1-x}C_x$ alloy supercells proceed by minimizing the lattice free energy computed via Eq. (1), by allowing the supercell lattice vectors and ionic positions to relax freely.

B. Tight-binding Hamiltonian

Given its use of a localized basis of atomic orbitals, the TB method is well suited to analyze the impact of localized impurities on the electronic structure of a given host matrix semiconductor.[52] This is of particular importance for highly-mismatched alloys—such as $Ge_{1-x}C_x$—in which the constituent elements have significant differences in size and chemical properties. We employ a nearest-neighbor sp^3s^* TB Hamiltonian,[53] based closely on that we have recently established for $Ge_{1-x}Sn_x$ alloys.[54] We note however that the TB model employed here differs from that of Ref. 54 in that we omit spin-orbit coupling. This is justified on the basis that DFT calculations have demonstrated that C incorporation in Ge primarily impacts the band structure close in energy to

the Ge CB edge,[24,27] where spin-orbit coupling has minimal impact. Henceforth, we therefore refer to high-symmetry eigenstates of Ge using the conventional O_h ($m\bar{3}m$) point group notation for the diamond lattice.[55]

It is well established that the accuracy of the TB fit to the band structure of a given semiconductor material can be improved via the inclusion of d-like atomic orbitals, to obtain a $sp^3s^*d^5$ basis set.[56] We have chosen to employ an sp^3s^* rather than $sp^3s^*d^5$ basis in our calculations for two reasons. First, while the $sp^3s^*d^5$ basis allows for more accurate fitting of a given target band dispersion, this comes at the cost of doubling the size of the Hamiltonian for a supercell containing a given number of atoms compared to that associated with a sp^3s^* basis. For the large supercell sizes required to simulate the properties of realistic highly-mismatched alloys, this doubling of the size of the supercell Hamiltonian represents a significant increase in the computational cost of numerical diagonalization. Second, while the $sp^3s^*d^5$ basis enables a more accurate fit to a range of band edge effective masses and higher energy CB states, the sp^3s^* basis is sufficient to accurately describe the band energies at high-symmetry points in the Brillouin zone. Since our aim here is to describe the nature of the alloy bandgap, we are interested primarily in C-induced band hybridization effects. The strength with which different eigenstates of a given semiconductor hybridize in response to a perturbation generally depends critically on the separation in energy of a small number of high-symmetry states. For dilute $Ge_{1-x}C_x$ alloys, we are interested in identifying the potential presence of an indirect- to direct-gap transition, so it is crucial that the energy of the L_{1c} (L-point CB minimum) states is described accurately relative to the $\Gamma_{2'c}$ (zone-center CB edge) state. For the purpose of describing the nature and evolution of the bandgap of a large number of semiconductor alloys, the sp^3s^* basis has been found to be sufficient, representing a small tradeoff in accuracy in order to significantly reduce parametric complexity and computational cost. Indeed, we have previously demonstrated that a TB Hamiltonian employing an sp^3s^* basis provides quantitatively accurate insight into the properties of highly-mismatched III-V semiconductor alloys containing nitrogen[57–59] (N), boron[60–62] (B), or bismuth[63–66] (Bi).

The impact of lattice relaxation (local strain) is incorporated in the TB Hamiltonian via bond length- and angle-dependent interatomic interaction matrix elements using, respectively, the generalized form of Harrison's rule[67,68] and the Slater-Koster two-center integrals.[69] To overcome the failure of this conventional parameterization to describe deformation potentials associated with tetragonal (biaxial) deformations, we include two additional strain-related terms. First, we include an on-site correction of the p orbital energies, which provides an accurate description of the Γ-point valence band (VB) edge axial deformation potential b.[70] Second, we include a correction to the $V_{s^*p\sigma}$ interatomic interaction matrix elements, which accounts for the influence of d orbital interactions in determining the axial deformation potential Ξ_u^X associated with the X-point CB edge states.[71] To incorporate these corrections in alloy supercell calculations we have cast them in local form, by writing the infinitesimal strain tensor at each lattice site in terms of the relaxed nearest-neighbor bond lengths and angles about that site. For a given relaxed alloy supercell, the construction of the supercell Hamiltonian—which accounts explicitly for size and chemical differences between constituent elements—proceeds as described in Ref. 54.

Our TB parameters are obtained by fitting to selected high-symmetry point energies determined via hybrid functional (HSEsol) DFT calculations.[45] Since C incorporation in Ge primarily impacts the band structure close in energy to the CB edge of the Ge host matrix semiconductor, our priority in fitting TB parameters for Ge was to describe the energies of the $\Gamma_{2'c}$, L_{1c}, and X_{1c} high-symmetry Γ-, L-, and X-point CB edge states.[54] For C and zb-GeC, we follow the fitting procedure outlined by Vogl *et al.*[53] without modification. Full details of the TB parameterization for $Ge_{1-x}C_x$ and related group-IV alloys will be presented in Ref. 45. The zero of energy for our alloy TB Hamiltonian is set at the Ge $\Gamma_{25'v}$ VB edge. We assume a natural VB offset of −4.24 eV between C and Ge, following the first principles calculations of Li *et al.*[72] Based on a linear interpolation of this VB offset with respect to the HSEsol-calculated lattice constants of C and Ge,[44] we estimate a VB offset of −2.12 eV between Ge and zb-GeC.

The resulting TB fits to the Ge, zb-GeC, and C band structures are shown, respectively, in Figs. 1(a), 1(b), and 1(c), where solid (dashed) black lines show the TB-calculated (reference HSEsol DFT[45]) band structure. Note the differences in scales on the ordinates of Figs. 1(a), 1(b), and 1(c). For zb-GeC and C, the underestimation of the L-point CB edge energies represents a typical sp^3s^* fit.[53] We note, however, that these discrepancies, which are largest in our TB fit to the band structure of C, should have minimal impact in alloy supercell calculations. Since we employ a nearest-neighbor TB Hamiltonian, parameters for C are only employed in the construction of the supercell Hamiltonian when C atoms appear as nearest neighbors. In a randomly disordered substitutional $Ge_{1-x}C_x$ alloy having C composition x, the probability for small x of two C atoms occupying nearest-neighbor lattice sites is $2x^2$—i.e., a randomly disordered N-atom $Ge_{1-x}C_x$ supercell will contain, on average, a total of $N \times 2x^2$ C–C nearest-neighbor pairs. Since we are concerned only with dilute C compositions $x \lesssim 2\%$, for the supercells considered in our analysis—which contain $N \leq 2000$ atoms—we expect < 2 C–C pairs to be present in any given disordered alloy supercell. This indeed turns out to be the case for the disordered supercells considered in Sec. III D, in which C atoms are substituted at statistically randomly selected lattice sites. In addition, as we describe in Sec. III A, the results of our TB supercell calculations for small, ordered $Ge_{1-x}C_x$ supercells are in good quantitative agreement with hybrid functional DFT calculations,[27,73] confirming the validity of our TB model to investigate $Ge_{1-x}C_x$ alloys.

III. RESULTS

In this section, we present the results of our analysis of the electronic structure of dilute $Ge_{1-x}C_x$. We begin in Sec. III A by considering the impact of C incorporation on the band structure of ordered alloy supercells, and then in Secs. III B and III C, we, respectively, analyze in detail the character and localization of the alloy CB edge states as a function of C composition x. Next, in Sec. III D, we turn our attention to the evolution of the electronic structure with x in realistic (large, disordered) alloy supercells.

Since the $Ge_{1-x}C_x$ band edge evolves from the L_{1c} CB minimum states of Ge, and since we are interested in the potential evolution of a direct bandgap in $Ge_{1-x}C_x$ alloys—whereby the alloy CB edge would acquire predominately Ge $\Gamma_{2'c}$ character—we

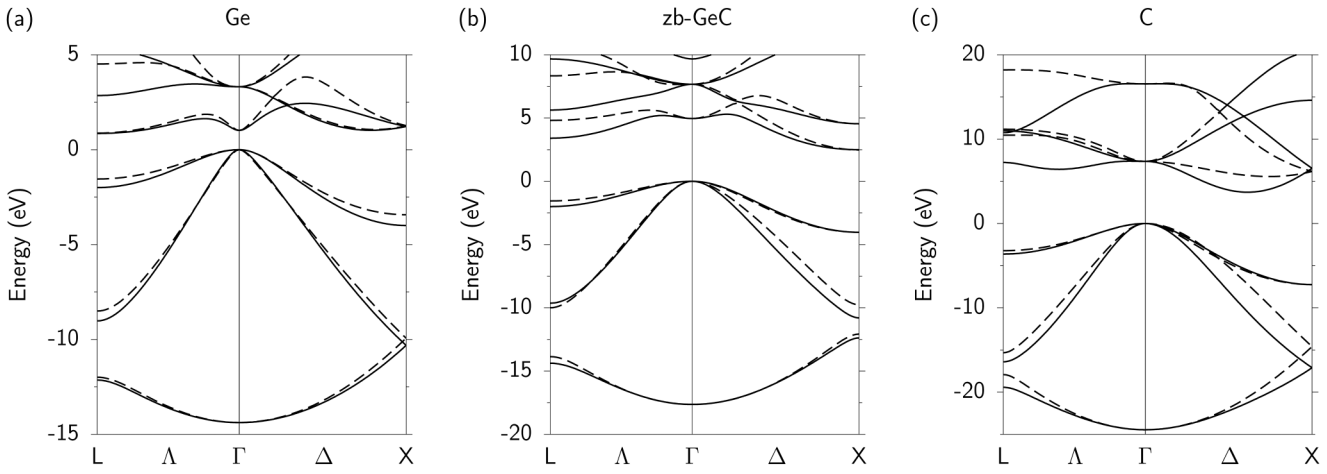

FIG. 1. Band structure of (a) Ge, (b) zb-GeC, and (c) C, calculated via DFT using the HSEsol exchange-correlation functional (dashed lines) and via a semiempirical sp^3s^* TB Hamiltonian (solid lines). All calculations omit spin-orbit coupling. For comparative purposes, the zero of energy has been chosen to lie at the Fermi level (VB edge) in all cases. Note the differences in scales on the ordinates of (a), (b), and (c).

restrict our attention primarily to supercells in which the L-point states of the underlying diamond structure fold to the supercell zone-center $\mathbf{K} = 0$—i.e., $n \times n \times n$ face-centered cubic (FCC) or simple cubic (SC) supercells for even values of n. This allows for C-induced hybridization of the L_{1c} CB minimum and $\Gamma_{2'c}$ zone-center CB edge states of Ge, which can be expected to be important given the small ≈ 0.15 eV separation in energy between the fundamental (indirect) and direct bandgaps of Ge. Indeed, we have recently demonstrated the importance of such effects in determining the nature of the indirect-to direct-gap transition in $Ge_{1-x}Sn_x$ and $Ge_{1-x}Pb_x$ alloys.[23,54,74] Our calculations suggest, in agreement with hybrid functional DFT calculations,[24,27] that C incorporation has minimal impact on the VB structure, so we focus our analysis on the alloy CB structure.

A. Band structure of ordered $Ge_{1-x}C_x$ alloy supercells

Figure 2(b) shows the calculated CB structure of an ordered, 128-atom $Ge_{127}C_1$ ($x = 0.78\%$) supercell. For comparative purposes, the CB structure of the corresponding C-free Ge_{128} supercell is shown in Fig. 2(a). The band dispersion is plotted as a function of the supercell wave vector $\mathbf{K}$ in units of $\frac{\pi}{A}$, where A is the supercell lattice constant, equal, respectively, to $\frac{na}{2}$ or na for an $n \times n \times n$ FCC or SC supercell. The lowest energy CB states at $\mathbf{K} = 0$ in Ge_{128} are the folded L_{1c} CB edge states, with the $\Gamma_{2'c}$ zone-center state lying 160 meV higher in energy. For the $Ge_{127}C_1$ supercell, we first note that C incorporation strongly perturbs the CB structure, leading to a large bandgap reduction of 91 meV compared to the fundamental bandgap of Ge ($E_g = 0.856$ eV, in the absence of spin-orbit coupling). Additionally, we note that the alloy CB minimum lies at $\mathbf{K} = 0$. Indeed, based on the qualitative inspection of Fig. 2(b), it is tempting to conclude—given the strong bandgap reduction and apparent emergence of a C-related impurity band lying energetically within the Ge bandgap—that C acts as an isovalent impurity, driving strong bandgap reduction via a BAC interaction, as suggested by Stephenson *et al.*[24,25] However, we note that the CB edge state is nondegenerate, while the second lowest energy set of CB states—lying 108 meV above the CB edge in energy—is threefold degenerate. This suggests C-induced splitting of the fourfold degenerate L_{1c} CB edge states of Ge, and that the alloy CB edge might be better described in terms of a linear combination of Ge L_{1c} states, rather than as a C-related localized impurity state.

To ascertain whether or not this is the case, we have undertaken a quantitative analysis of the character of the alloy CB states. Figure 2(c) shows the fractional Ge $\Gamma_{2'c}$ character of the $Ge_{127}C_1$ CB states, calculated by projecting the $\Gamma_{2'c}$ eigenstate $|\Gamma^{(0)}_{2'c}\rangle$ of the Ge_{128} host matrix supercell onto the full spectrum $\{|n(x)\rangle\}$ of $\mathbf{K} = 0$ $Ge_{127}C_1$ alloy CB eigenstates. Note that we use the superscript "(0)" henceforth to denote unperturbed Ge host matrix eigenstates. We calculate that the $Ge_{127}C_1$ CB edge eigenstate—highlighted in Fig. 2(c) via green coloring—acquires a small (12.0%) admixture of Ge $\Gamma_{2'c}$ character. As a consequence of their symmetry, the second lowest energy set of CB states acquire no Ge $\Gamma_{2'c}$ character, while the third lowest energy state—originating from the Ge $\Gamma_{2'c}$ state and lying 296 meV above the alloy CB edge in energy—retains majority (54.4%) Ge $\Gamma_{2'c}$ character. We find that the remainder of the Ge $\Gamma_{2'c}$ character is spread over a small number of higher energy alloy CB states, originating primarily from the folded X_{1c} CB edge states of Ge. Our calculations therefore suggest that the $Ge_{127}C_1$ CB edge acquires only minimal direct (Ge $\Gamma_{2'c}$) character. To confirm this, we calculate the pressure coefficient $\frac{dE_g}{dP}$ associated with the fundamental bandgap. We have demonstrated elsewhere[23,54,74] that calculation of alloy band structure as a function of hydrostatic pressure can provide useful quantitative insight into the character of the band edge states, and hence the nature and evolution of the alloy bandgap. The pressure coefficients associated the indirect L_{1c}-$\Gamma_{25'v}$, direct $\Gamma_{2'c}$-$\Gamma_{25'v}$, and indirect X_{1c}-$\Gamma_{25'v}$ bandgaps of Ge are significantly different to one another, having respective values $\frac{dE_g}{dP} = 13.33$, 4.66, and -1.60 meV kbar^{-1} in the HSEsol DFT calculations to which we

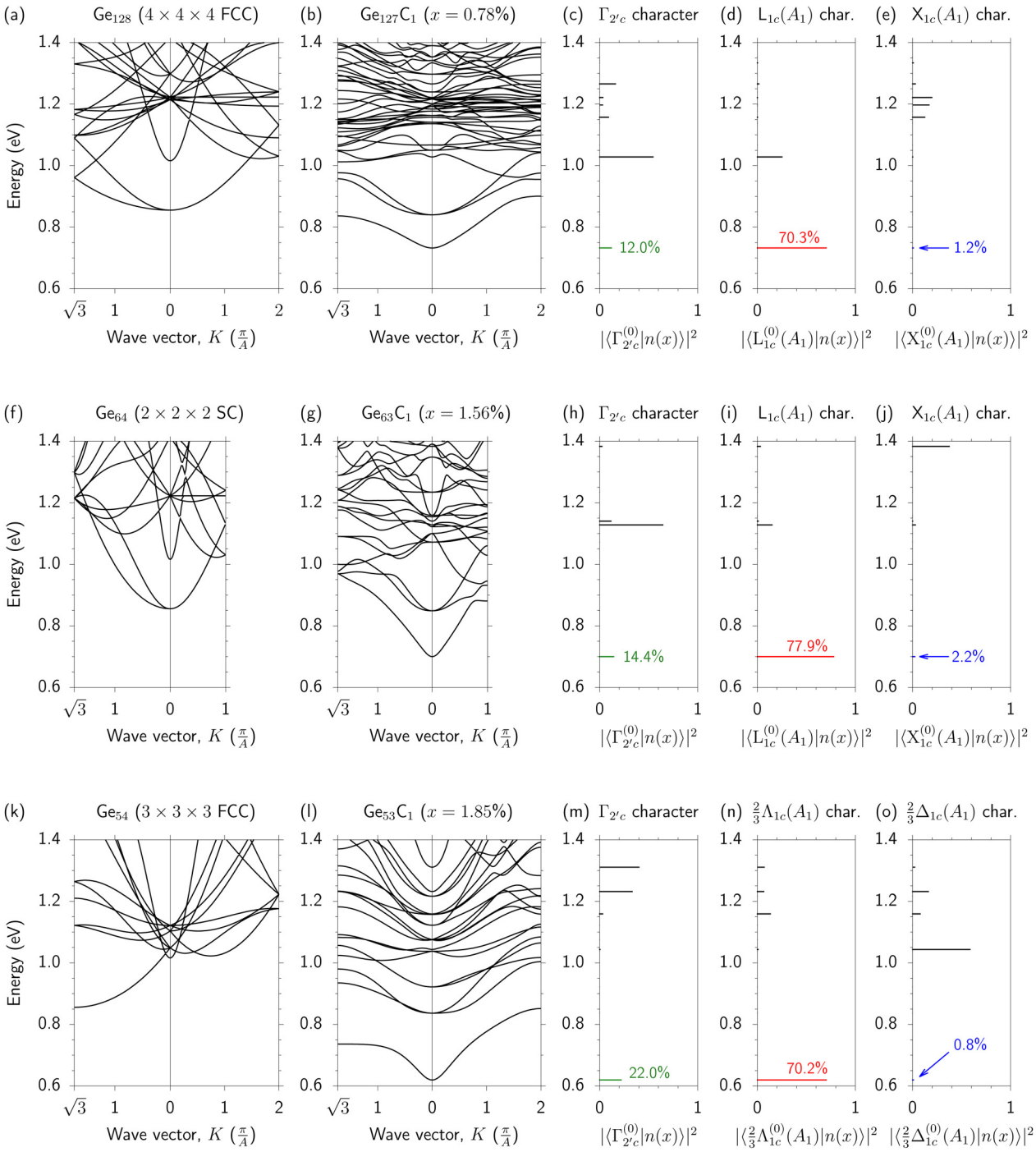

FIG. 2. Top row: Calculated CB structure for (a) a C-free Ge_{128} supercell, and (b) an ordered $Ge_{127}C_1$ ($x = 0.78\%$) supercell. (c)–(e), respectively, show the calculated fractional Ge $\Gamma_{2'c}$, $L_{1c}(A_1)$, and $X_{1c}(A_1)$ character spectra of the $Ge_{127}C_1$ supercell of (b). Middle row: Calculated CB structure for (f) a C-free Ge_{64} supercell and (g) an ordered $Ge_{63}C_1$ ($x = 1.56\%$) supercell. (h)–(j), respectively, show the calculated fractional Ge $\Gamma_{2'c}$, $L_{1c}(A_1)$, and $X_{1c}(A_1)$ character spectra for the $Ge_{63}C_1$ supercell of (g). Bottom row: Calculated CB structure for (k) a C-free Ge_{54} supercell and (l) an ordered $Ge_{53}C_1$ ($x = 1.85\%$) alloy supercell. (m)–(o), respectively, show the calculated fractional Ge $\Gamma_{2'c}$, $\frac{2}{3}\Lambda_{1c}(A_1)$ and $\frac{2}{3}\Delta_{1c}(A_1)$ character spectrum for the $Ge_{53}C_1$ supercell of (l). The zero of energy of all band structure plots is set at the Ge VB edge. Green, red, and blue coloring is used to highlight the Ge $\Gamma_{2'c}$, $L_{1c}(A_1)$ (or $\frac{2}{3}\Lambda_{1c}(A_1)$), and $X_{1c}(A_1)$ [or $\frac{2}{3}\Delta_{1c}(A_1)$] character of the CB edge state in each alloy supercell.

fit our TB parameters. Since we are dealing with dilute C compositions, we expect that an alloy having primarily indirect character will have a significantly lower pressure coefficient than an alloy having direct-gap character. We calculate $\frac{dE_g}{dP} = 5.25$ meV kbar^{-1} for the $Ge_{127}C_1$ supercell confirming that, despite strong perturbation of the CB structure, the alloy CB edge retains primarily Ge L_{1c} character. Our calculated value of $\frac{dE_g}{dP}$ here is in good agreement with the value of 4.55 meV kbar^{-1} obtained from the hybrid functional DFT calculations of Ref. 27.

Direct inspection of the $Ge_{127}C_1$ CB edge eigenstate reveals purely *s*-like orbital character (A_1 symmetry) at the C lattice site. Since, in general, alloying drives hybridization between host matrix states having the same symmetry, we conclude that C incorporation drives hybridization primarily between $|\Gamma^{(0)}_{2'c}\rangle$ and a linear combination $|L^{(0)}_{1c}(A_1)\rangle$ of Ge L_{1c} eigenstates having purely *s*-like orbital character at the C lattice site. We confirm that this is the case by using the $\mathbf{K} = 0$ eigenstates of a C-free Ge_{128} supercell to explicitly construct $|L^{(0)}_{1c}(A_1)\rangle$, and then calculate the corresponding Ge $L_{1c}(A_1)$ character of the $Ge_{127}C_1$ CB states—shown in Fig. 2(d)—analogously to the calculation of the $\Gamma_{2'c}$ character. Doing so, we indeed find that the $Ge_{127}C_1$ CB edge eigenstate—highlighted in Fig. 2(d) via red coloring—is constituted primarily of $|L^{(0)}_{1c}(A_1)\rangle$, having 70.3% Ge $L_{1c}(A_1)$ character. Finally, since the calculated Ge $\Gamma_{2'c}$ and $L_{1c}(A_1)$ character of Figs. 2(c) and 2(d) demonstrates the presence of hybridization between $\Gamma_{2'c}$, $L_{1c}(A_1)$ and higher energy CB states, we investigate the possibility of C-induced mixing with higher energy Ge host matrix CB states. In Ge_{128}, the next highest energy CB states above $\Gamma_{2'c}$ are the folded X_{1c} CB edge states. As such, we construct $|X^{(0)}_{1c}(A_1)\rangle$—i.e., a linear combination of Ge X_{1c} states having purely *s*-like orbital character at the C lattice site—and calculate the Ge $X_{1c}(A_1)$ character of the $Ge_{127}C_1$ CB states. The results of this analysis are shown in Fig. 2(e), where we note that the $Ge_{127}C_1$ CB edge eigenstate—highlighted in Fig. 2(e) via blue coloring—acquires only 0.8% Ge $X_{1c}(A_1)$ character. We therefore conclude for the $Ge_{127}C_1$ supercell considered here (i) that C incorporation drives hybridization between A_1-symmetric Ge host matrix states lying close in energy to the CB edge, (ii) that the $Ge_{127}C_1$ CB edge is derived primarily from a linear combination $|L^{(0)}_{1c}(A_1)\rangle$ of Ge L_{1c} CB minimum states, and (iii) that the alloy bandgap retains primarily indirect character.

To investigate these trends as a function of x, we have repeated this analysis for an ordered, 64-atom $Ge_{63}C_1$ ($x = 1.56\%$) supercell, the calculated CB structure of which is shown in Fig. 2(g). The CB structure of the corresponding C-free Ge_{64} supercell is shown in Fig. 2(f). Again, we note that the lowest energy CB states at $\mathbf{K} = 0$ in Ge_{64} are the folded L_{1c} CB minimum states. Since this supercell has SC lattice vectors, the Brillouin zone boundary along (001) lies at $K_z = \frac{\pi}{A}$. Again, we note that C incorporation leads to a strong reduction of the bandgap, by 93 meV compared to the fundamental bandgap of Ge. Despite that the C composition in $Ge_{63}C_1$ is twice that in $Ge_{127}C_1$, we note that the calculated bandgap reduction in both cases is approximately equal. This suggests strong composition-dependent bowing of the alloy bandgap, the details of which depend precisely on the band mixing (hybridization) present in a given alloy supercell. We note that the ordering, degeneracy, and orbital character of the $Ge_{63}C_1$ $\mathbf{K} = 0$ eigenstates are as described above for $Ge_{127}C_1$. Figures 2(h), 2(i), and 2(j) show, respectively, the Ge $\Gamma_{2'c}$, $L_{1c}(A_1)$ and $X_{1c}(A_1)$ character of the $Ge_{63}C_1$ $\mathbf{K} = 0$ CB states. Qualitatively, we note similar trends as for the $Ge_{127}C_1$ supercell. First, C incorporation drives hybridization between the $\Gamma_{2'c}$, L_{1c}, and X_{1c} states of the Ge host matrix. Second, the alloy CB edge eigenstate retains primarily (77.9%) indirect [Ge $L_{1c}(A_1)$] character and acquires only a small admixture (14.4%) of direct (Ge $\Gamma_{2'c}$) character. As in Figs. 2(c)–2(e), the $\Gamma_{2'c}$, $L_{1c}(A_1)$, and $X_{1c}(A_1)$ character of the $Ge_{63}C_1$ CB edge eigenstate in Figs. 2(h)–2(j) is highlighted using green, red, and blue coloring. Thirdly, C-induced hybridization between Ge $\Gamma_{2'c}$ and X_{1c} states is negligible, with the alloy CB edge state acquiring only minimal (2.2%) Ge $X_{1c}(A_1)$ character.

We have so far considered the impact of C incorporation on the CB edge states only in the case where the L-point eigenstates of the corresponding C-free Ge supercell fold to $\mathbf{K} = 0$. It is, however, pertinent to enquire as to whether the trends identified above—and hence our conclusion that the $Ge_{1-x}C_x$ bandgap retains primarily indirect character—is a consequence of the choice of supercells employed in our analysis. Indeed, the mechanism driving the electronic structure evolution in response to C incorporation should be present in all alloy supercells, regardless of the specific choice of supercell. To address this issue, we present also the results of equivalent analysis for an ordered, 54-atom $Ge_{53}C_1$ ($x = 1.85\%$) supercell, the calculated CB structure of which is shown in Fig. 2(l). The CB structure of the corresponding C-free Ge_{54} supercell is shown in Fig. 2(k). For this $3 \times 3 \times 3$ FCC supercell, the L points of the Brillouin zone of the underlying diamond lattice map directly to the L points of the supercell Brillouin zone. As such, the calculated CB minimum in Ge_{54} lies at $\mathbf{K} = (\frac{\pi}{A}, \frac{\pi}{A}, \frac{\pi}{A})$. Comparing Figs. 2(k) and 2(l), we note that, qualitatively, the impact of C incorporation on the CB edge again appears to illustrate the emergence of a direct bandgap: the CB minimum relocates from $\mathbf{K} = (\frac{\pi}{A}, \frac{\pi}{A}, \frac{\pi}{A})$ to $\mathbf{K} = 0$ in response to C incorporation. Figure 2(m) shows the calculated Ge $\Gamma_{2'c}$ character of the $Ge_{53}C_1$ $\mathbf{K} = 0$ CB states. We note that the alloy CB edge again acquires only minority (22.0%) Ge $\Gamma_{2'c}$ character. Despite the explicit choice of a Ge host matrix supercell in which the CB minimum is not folded to $\mathbf{K} = 0$ [cf. Fig. 2(k)], giving way to a C-containing alloy supercell CB structure having its minimum at $\mathbf{K} = 0$ [cf. Fig. 2(l)], careful analysis of the corresponding supercell CB edge eigenstate reveals primarily indirect character.

In this 54-atom supercell, hybridization between the Ge $\Gamma_{2'c}$ and L_{1c} states is blocked, since the latter do not fold back to $\mathbf{K} = 0$. In Ge_{54}, the lowest energy CB states that fold to $\mathbf{K} = 0$ originate from wave vectors $\mathbf{k} = (\frac{2\pi}{3a}, \frac{2\pi}{3a}, \frac{2\pi}{3a})$, and equivalent points, located two-thirds of the way along the Λ direction between the Γ and L points in the primitive cell Brillouin zone of the underlying diamond lattice. These states which we denote by $|\frac{2}{3}\Lambda^{(0)}_{1c}\rangle$, lie 33 meV above the $\Gamma_{2'c}$ zone-center CB edge state in Fig. 2(k). The next lowest energy set of Ge states which fold to $\mathbf{K} = 0$ originate from wave vectors $\mathbf{k} = (0, 0, \frac{4\pi}{3a})$, and equivalent points, which lie two-thirds of the way along the Δ direction in the primitive cell Brillouin zone. The corresponding $\mathbf{K} = 0$ states in Ge_{54}, which we denote by $|\frac{2}{3}\Delta^{(0)}_{1c}\rangle$, lie 88 meV above the $\Gamma_{2'c}$ zone-center CB edge states. Figures 2(n) and 2(o), respectively, show the corresponding calculated Ge $\frac{2}{3}\Lambda_{1c}(A_1)$ and $\frac{2}{3}\Delta_{1c}(A_1)$ character of the $Ge_{53}C_1$ $\mathbf{K} = 0$ CB eigenstates. The Ge $\Gamma_{2'c}$, $\frac{2}{3}\Lambda_{1c}(A_1)$ and $\frac{2}{3}\Delta_{1c}(A_1)$ character of the CB edge eigenstate is highlighted in Figs. 2(m)–2(o)

using green, red, and blue coloring, respectively. We calculate that the CB edge eigenstate has majority (70.2%) Ge $\frac{2}{3}\Lambda_{1c}(A_1)$ character and acquires only minimal (0.8%) Ge $\frac{2}{3}\Delta_{1c}(A_1)$ character. We note the quantitative similarity to the $Ge_{127}C_1$ and $Ge_{63}C_1$ cases: despite that the L- and X-points do not fold to $\mathbf{K} = 0$ in Ge_{54}, the $Ge_{53}C_1$ is nonetheless formed primarily of a linear combination of states originating from a point along the Λ direction in the primitive cell Brillouin zone, which possesses purely *s*-like orbital character at the C lattice site. Overall, we therefore conclude that the CB edge eigenstate in ordered $Ge_{1-x}C_x$ alloys retains primarily indirect character, irrespective of the specific choice of supercell(s) employed in electronic structure calculations. As such, we consequently conclude that C incorporation does not drive the formation of a direct band gap in dilute $Ge_{1-x}C_x$. This conclusion is in direct agreement with the hybrid functional DFT calculations of Kirwan *et al.*[27]

B. Trends vs C composition: Band mixing and the ultradilute (impurity) limit

Having investigated in detail the impact of C incorporation in small ordered supercells containing ≤ 128 atoms, we turn our attention now to the evolution of the alloy CB edge state and bandgap as we approach the ultradilute limit of having an isolated substitutional C atom in a Ge matrix. The results of these calculations are summarized in Fig. 3, which shows the calculated variation with x of (a) the bandgap reduction ΔE_g (upper panel) and bandgap pressure coefficient $\frac{dE_g}{dP}$ (lower panel) and (b) the Ge $\Gamma_{2'c}$ character (upper panel) and Ge $L_{1c}(A_1)$ (lower panel) character of the $\mathbf{K} = 0$ CB edge eigenstate. Results are shown for ordered $Ge_{N-1}C_1$ supercells containing $16 \leq N \leq 2000$ atoms: the lowest (highest) C composition investigated is $x = 0.05\%$ ($x = 6.25\%$) in an ordered $10 \times 10 \times 10$ FCC $Ge_{1999}C_1$ ($2 \times 2 \times 2$ FCC $Ge_{15}C_1$) supercell. Results for $n \times n \times n$ supercells having even (odd) values of n are denoted in Figs. 3(a) and 3(b) by closed (open) circles. We recall that for odd n supercells, the L points of the primitive cell Brillouin zone associated with the underlying diamond lattice do not fold to $\mathbf{K} = 0$ so that C-induced $\Gamma_{2'c}$-L_{1c} hybridization is blocked.

Examining Fig. 3(a) we note that, in general, C incorporation drives a strong reduction of the $\mathbf{K} = 0$ supercell bandgap, with the magnitude of the bandgap reduction ΔE_g growing strongly with increasing x (decreasing N). The lowest bandgap we calculate is $E_g = 0.599$ eV in a $Ge_{15}C_1$ supercell, which is reduced by 257 meV compared to the fundamental (indirect) bandgap of Ge. For some large (ultradilute) supercells, we calculate a zone-center bandgap which exceeds the fundamental L_{1c}-$\Gamma_{25'v}$ bandgap of the Ge host matrix. We emphasize that this is a result of the L_{1c} states not folding to $\mathbf{K} = 0$ in these supercells: the lowest energy CB states in these supercells originate from wave vectors $\mathbf{k} = (\frac{2\pi}{na}, \frac{2\pi}{na}, \frac{2\pi}{na})$ located two-*n*ths of the way along the Λ direction in the primitive unit cell Brillouin zone, and hence lie higher in energy than the L_{1c} CB minima. For sufficiently low x, C-induced hybridization of A_1-symmetric Ge CB edge states is insufficient to push the fundamental bandgap below that of Ge. Closed red squares in the bottom panel of Fig. 3(a) show the values of $\frac{dE_g}{dP}$ calculated via hybrid functional DFT by Kirwan *et al.*[27] Generally, we find that our TB-calculated pressure coefficients are $\approx$1 meV kbar^{-1} larger than those obtained from equivalent hybrid functional DFT calculations. This indicates a tendency of the TB calculations to overestimate the Ge $\Gamma_{2'c}$ character associated with the $Ge_{1-x}C_x$ alloy CB edge, emphasizing the robustness of our conclusions regarding the indirect nature of the alloy

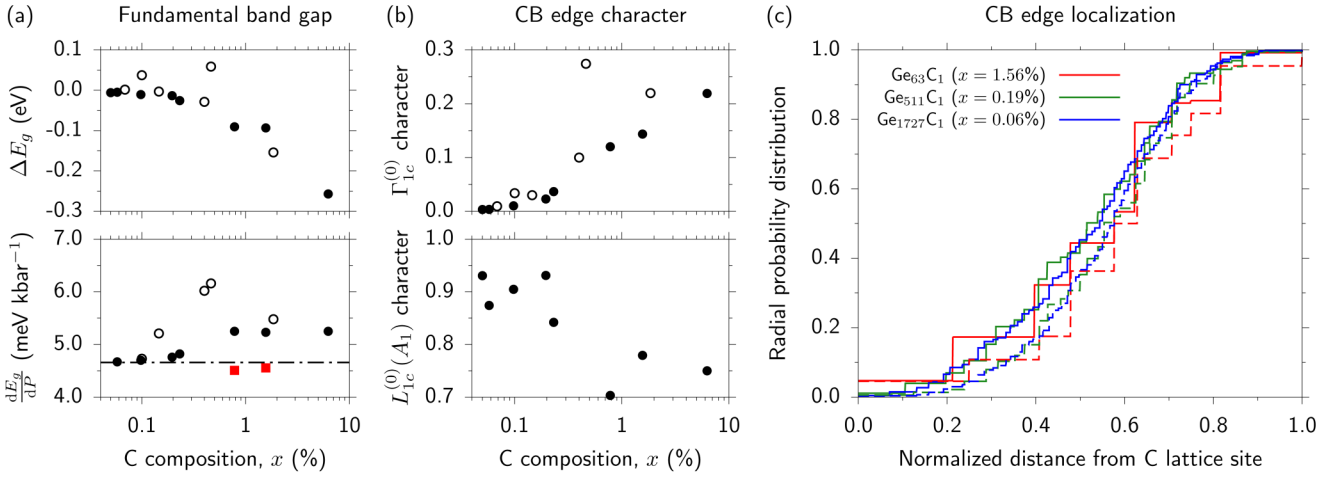

FIG. 3. (a) Change in $\mathbf{K} = 0$ bandgap ΔE_g (upper panel) and bandgap pressure coefficient $\frac{dE_g}{dP}$ (lower panel) as a function of C composition x for a series of ordered $Ge_{N-1}C_1$ ($x = \frac{1}{N}$) alloy supercells containing $16 \leq N \leq 2000$ atoms. The dashed gray line in the lower panel denotes the pressure coefficient $\frac{dE_g}{dP} = 4.66$ meV kbar^{-1} of the fundamental (indirect) bandgap of Ge. The closed red squares in the lower panel show the hybrid functional DFT-calculated values of $\frac{dE_g}{dP}$ from Ref. 27. (b) Fractional Ge $\Gamma_{2'c}$ (upper panel) and $L_{1c}(A_1)$ (lower panel) character of the alloy CB edge eigenstate for the same ordered $Ge_{N-1}C_1$ supercells as in (a). Closed (open) circles in (a) and (b) correspond to $n \times n \times n$ FCC or SC supercells having even (odd) values of n. (c) Radial probability distribution functions (RPDFs) for the CB edge eigenstate in ordered $Ge_{63}C_1$ (solid red line), $Ge_{511}C_1$ (solid green line), and $Ge_{1727}C_1$ (solid blue line) supercells. In each case, the dashed line of the same color shows the calculated RPDF for the CB edge eigenstate $|L^{(0)}_{1c}(A_1)\rangle$ of the corresponding Ge_N host matrix supercell.

bandgap. Turning our attention to the lower part of Fig. 3(b), we again note that the precise calculated value of $\frac{dE_g}{dP}$ depends on the specific details of band hybridization—as determined by zone folding—in a given alloy supercell. For all supercells, the calculated values of $\frac{dE_g}{dP}$ remain significantly closer to the value 4.66 meV kbar^{-1} associated with the L_{1c}-$\Gamma_{25'v}$ indirect bandgap of Ge than to the value 13.33 meV kbar^{-1} associated with the direct $\Gamma_{2'c}$-$\Gamma_{25'v}$ bandgap. This emphasizes that the $Ge_{1-x}C_x$ bandgap retains primarily indirect character, even for C compositions as high as $x = 6.25\%$.

The indirect nature of the $Ge_{1-x}C_x$ bandgap is further emphasized by analyzing the evolution of the calculated Ge $\Gamma_{2'c}$ and $L_{1c}(A_1)$ character of the $Ge_{N-1}C_1$ CB edge eigenstates, shown, respectively, in the upper and lower panels of Fig. 3(b). Note the absence of open circles in the lower panel of Fig. 3(b): since the L-point eigenstates in an odd n supercell do not fold to $\mathbf{K} = 0$, the Ge L_{1c} eigenstates cannot contribute to the $\mathbf{K} = 0$ supercell eigenstates. As x decreases (N increases) toward the ultradilute limit, we note that the CB edge Ge $\Gamma_{2'c}$ character tends toward zero. Similarly, we note that the CB edge Ge $L_{1c}(A_1)$ character tends to increase with decreasing x. While the CB edge Ge $\Gamma_{2'c}$ character reaches a value as low as 0.3% in the largest ($Ge_{1999}C_1$) supercell considered, we note that the corresponding Ge $L_{1c}(A_1)$ character attains a value 93.1% in the same supercell. This reflects that, for the case of an isolated substitutional C atom, the CB edge state consists primarily of a linear combination of Ge L_{1c} states having A_1 symmetry at the C lattice site, and also possesses a small admixture of other (non-$\Gamma_{2'c}$) A_1-symmetric linear combinations of Ge states. The largest calculated alloy CB edge Ge $\Gamma_{2'c}$ character in an even n supercell is 21.9% in $Ge_{15}C_1$ ($x = 6.25\%$), suggesting that $Ge_{1-x}C_x$ acquires minimal direct-gap character even as the C composition is increased beyond the dilute regime. We note higher Ge $\Gamma_{2'c}$ character in the 216-atom $Ge_{215}C_1$ ($x = 0.46\%$) supercell, but recall from Fig. 3(a) that the lowest energy CB state at $\mathbf{K} = 0$ in this supercell lies above the Ge L_{1c} CB edge, with the resultant reduced separation in energy between the folded Ge_{216} CB edge and the $\Gamma_{2'c}$ state driving strong hybridization in a 216-atom alloy supercell.

For small ($N \leq 128$) supercells, we note that our calculated values of ΔE_g and $\frac{dE_g}{dP}$ are in good quantitative agreement with the hybrid DFT calculations of Ref. 27. Our calculated CB structure for an ordered $Ge_{127}C_1$ supercell is also in good overall agreement with the calculations of Kirwan *et al.*,[27] as well as those of Stephenson *et al.*[25] At higher C compositions, our calculations disagree qualitatively with the hybrid DFT calculations of Ref. 25, which suggest that the alloy bandgap has closed even in a $Ge_{53}C_1$ ($x = 1.85\%$) supercell. We note, however, that the $Ge_{53}C_1$ supercell band structure presented in Ref. 25 contains several unusual features, including a large energy splitting of the VB edge states. This VB edge splitting, which should vanish in an ordered alloy supercell, suggests improper supercell relaxation, casting doubt on the suggestion that the bandgap closes in the C composition range between 1.56% (in $Ge_{63}C_1$) and 1.85% (in $Ge_{53}C_1$).

C. Evolution of conduction band edge eigenstates in ordered alloy supercells

Having considered in detail the character of the CB edge eigenstates, we finally consider the potential for carrier localization in response to C incorporation. The solid red, green, and blue lines in Fig. 3(c), respectively, show the calculated cumulative radial probability distribution function (RPDF) associated with the CB edge eigenstates in $Ge_{63}C_1$ ($x = 1.56\%$), $Ge_{511}C_1$ ($x = 0.19\%$), and $Ge_{1727}C_1$ ($x = 0.06\%$)—i.e., $2 \times 2 \times 2$, $4 \times 4 \times 4$, and $6 \times 6 \times 6$ SC—supercells. Here, the cumulative RPDF is calculated for a given supercell eigenstate by selecting the C lattice site as the origin of coordinates and then, at a given distance from this origin, adding the total probability density residing on atoms located at that distance from the C lattice site. For a given supercell eigenstate, the rate at which the cumulative RPDF approaches a value of unity gives an indication of the degree of localization of the state. As such, for an eigenstate strongly localized about the C lattice site, we would expect the calculated cumulative RPDF in Fig. 3(c) to rapidly approach a value of unity with increasing distance. To facilitate comparison of RPDFs calculated for eigenstates of supercells having different size, we plot the RPDF as a function of distance normalized to the maximum interatomic distance in each supercell—i.e., normalized by the dimensions of a given supercell. For a highly localized alloy CB edge state, we would then expect the cumulative RPDF to approach unity more rapidly with increasing supercell size in Fig. 3(c).

To quantify the presence of any localization generated by C incorporation, we show also in Fig. 3(c) the cumulative RPDFs associated with the constructed host matrix CB edge eigenstate $|L_{1c}^{(0)}(A_1)\rangle$ for the Ge_{64} (dashed red line), Ge_{512} (dashed green line), and Ge_{1728} (dashed blue line) supercells. We note that these $|L_{1c}^{(0)}(A_1)\rangle$ host matrix CB edge states extend through the full supercell: in a given N-atom Ge_N supercell, the associated cumulative RPDF, therefore, increases smoothly in magnitude with increasing distance from the lattice site on which the eigenstate has been constructed to have purely s-like orbital character. Considering first the cumulative RPDF associated with the Ge_{64} CB edge eigenstate, we calculate that 10% of the probability density associated with $|L_{1c}^{(0)}(A_1)\rangle$ resides on the origin and its four nearest-neighbor lattice sites. Substituting the Ge atom at the origin by C, this increases to 18% for the corresponding $Ge_{63}C_1$ ($x = 1.56\%$) supercell. Based solely on analysis of small supercell eigenstates, it then appears that C incorporation generates appreciable electron localization at the CB edge. However, this trend is not borne out in the larger supercells: in both $Ge_{511}C_1$ and $Ge_{1727}C_1$, we calculate that the associated increase in localization compared to the $|L_{1c}(A_1)\rangle$ host matrix CB edge state is $< 5\%$.

To quantify the overall change in localization in response to C incorporation, we have also calculated the inverse participation ratio (IPR) associated with the CB edge eigenstates in all supercells studied.[75,76] The IPR associated with an eigenstate in an N-atom supercell attains a minimum value of $\frac{1}{N}$ for a fully delocalized eigenstate having equal probability density at each lattice site, and a maximum value of 1 for a fully localized eigenstate for which the probability density resides entirely at a single lattice site. The calculated IPR for the $Ge_{N-1}C_1$ CB edge eigenstate tends toward an average value $\approx \frac{2}{N}$ in the ultradilute limit, a minimal increase from the value $\frac{1.62}{N}$ calculated for the corresponding $|L_{1c}^{(0)}(A_1)\rangle$ host matrix eigenstate. Similar analysis for higher energy alloy CB states reveals qualitatively similar results: incorporation of an isolated substitutional C atom in Ge does not lead to any significant electron localization about the C atom. (As we will describe in Sec. III D below, this is no longer the case in the presence of C

clustering, which can result in significant localization of electrons occupying states lying energetically within the Ge bandgap.)

The strong CB edge localization observed in calculations for small ordered $Ge_{N-1}C_1$ supercells[27] therefore gives way to a delocalized alloy CB edge in the ultradilute (large N) limit. This is in stark contrast to equivalent analysis of dilute nitride $GaN_x(As,P)_{1-x}$ alloys,[77,78] to which $Ge_{1-x}C_x$ has recently been compared, where substitutional N incorporation generates N-related impurity states, which are found to be highly localized about the N lattice site in the ultradilute limit. Based on the calculated high Ge $L_{1c}(A_1)$ character of the $Ge_{1-x}C_x$ CB edge eigenstates [cf. Figs. 2(d) and 2(i)], this lack of strong localization is not surprising: the alloy CB edge is formed primarily from a linear combination of a small number of delocalized Ge eigenstates and is hence itself delocalized. As such, we conclude that dilute C incorporation in Ge does not introduce significant electron localization about substitutional C atoms, which are spaced widely apart in ordered alloy supercells.

On the basis of our analysis of the electronic structure of ordered $Ge_{1-x}C_x$ alloy supercells, we conclude overall that—despite the large mismatch in size and chemical properties between Ge and C—from the perspective of the electronic structure an isolated C atom does not act as an isovalent impurity when incorporated substitutionally in Ge. Our analysis explicitly rules out the interpretation of the $Ge_{1-x}C_x$ CB structure in terms of C-related localized impurity states and the BAC model. Moreover, our analysis therefore suggests—in agreement with the conclusions of Kirwan *et al.*[27]—that substitutional C incorporation in Ge does not drive the formation of a direct bandgap in dilute $Ge_{1-x}C_x$ alloys.

D. Impact of C incorporation on conduction band edge states in disordered $Ge_{1-x}C_x$ alloys

Having quantified the impact of C incorporation on the electronic structure of ordered $Ge_{1-x}C_x$ alloy supercells, we turn our attention now to more realistic, disordered alloy supercells. To analyze the electronic structure in the presence of alloy disorder, two key requirements guide our choice of supercells. First, we must choose sufficiently large supercells so that incorporation of dilute C compositions $x \sim 1\%$ correspond to substitution of multiple C atoms. This allows for the formation of disordered local neighbor environments in the supercell and hence allows alloy disorder effects to be explicitly included in our electronic structure calculations. Second, since we have identified that C incorporation drives hybridization between Ge host matrix states lying close in energy to the CB edge, it is important that we choose supercells that accurately reflect this band mixing as it occurs in a real $Ge_{1-x}C_x$ alloy. In supercell calculations, more states fold back to $\mathbf{K} = 0$ close in energy to the CB edge as the supercell size increases, providing a more accurate representation of C-induced band hybridization. Based on the analysis of Sec. III B—showing that the electronic properties associated with an isolated C impurity have converged for $N \approx 2000$ atoms in the supercell—we, therefore, use 1728-atom ($6 \times 6 \times 6$ SC) $Ge_{1728-M}C_M$ ($x = \frac{M}{1728}$) supercells and perform calculations for supercells containing up to $M = 35$ substitutional C atoms ($x \approx 2\%$). To obtain a reliable description of the evolution of the electronic structure with x, we perform a high-throughput analysis: at each C composition we construct, relax and calculate the electronic structure of 25 distinct disordered supercells, where Ge atoms are substituted by C at randomly selected lattice sites. Results for a given C composition are then obtained via configurational averaging—i.e., by averaging over the results of calculations for these 25 distinct disordered supercells.

The configurational averaging approach is favorable here compared to the use of a single, ultralarge supercell at each distinct C composition, due to the localized nature of the alloy CB states in disordered $Ge_{1-x}C_x$ alloys (described below). In conventional semiconductor alloys, which display minimal carrier localization, eigenstate formation arises from the (generally weak) hybridization of delocalized eigenstates, therefore requiring ultralarge supercells to quantitatively describe the resultant alloy properties by directly encapsulating the associated length scales.[79] Conversely, highly-mismatched alloys are characterized by effects pertaining to carrier localization and short-range alloy disorder, which act on significantly reduced length scales.[42,80–82] Supercells containing $N \sim 10^3$ atoms are, therefore, sufficient to describe the properties of such materials, with configurational averaging providing an efficient means to explore the impact of the formation of distinct short-range (near-neighbor) environments on the electronic structure.[64,65,80,83]

As in Secs. III A–III C above, our primary concern is to quantify the evolution of the character of the alloy CB states with increasing x. To do this, we use the $\Gamma_{2'c}$ and folded L_{1c} states $|\Gamma_{2'c}^{(0)}\rangle$ and $|L_{1c}^{(0)}\rangle$ of the Ge_{1728} host matrix supercell to calculate the fractional Ge $\Gamma_{2'c}$ and L_{1c} character spectra of the $Ge_{1728-M}C_M$ $\mathbf{K} = 0$ CB eigenstates. To average the calculated spectra at fixed x, we sort the calculated Ge $\Gamma_{2'c}$ and L_{1c} character into energy intervals of width 5 meV: for each distinct disordered supercell, a given energy interval is populated by the total Ge $\Gamma_{2'c}$ or L_{1c} character of alloy CB states lying in the range of energy spanned by the interval, and the resulting totals for all 25 supercells are then averaged to obtain the average Ge $\Gamma_{2'c}$ or L_{1c} character in that energy range. The results of this analysis are summarized in Figs. 4(a)–4(h), which show the calculated evolution with x of the averaged fractional Ge $\Gamma_{2'c}$ (green) and L_{1c} (orange) character for the disordered 1728-atom $Ge_{1-x}C_x$ supercells described above. The C compositions in Fig. 4 begin at $x = 0$ for the C-free Ge_{1728} host matrix supercell in Fig. 4(a) and increase in steps of $M = 5$ C atoms in subsequent panels up to a maximum C composition $x = 2.03\%$ ($M = 35$) in Fig. 4(h). Note the different scales on the abscissae of Figs. 4(a), 4(b), and 4(c)–4(h).

Beginning in Fig. 4(a) with the reference Ge_{1728} supercell, the lowest energy $\mathbf{K} = 0$ CB states are the fourfold degenerate folded L_{1c} states that possess 100% Ge L_{1c} character, while the next lowest energy CB state is the $\Gamma_{2'c}$ state that possesses 100% Ge $\Gamma_{2'c}$ character. Next, Fig. 4(b) shows the corresponding spectra calculated and averaged for $Ge_{1723}C_5$ ($x = 0.29\%$) supercells. We first observe, as in our ordered supercell calculations (cf. Sec. III A), that C incorporation generates a downward shift in energy of CB states possessing Ge L_{1c} character, reflecting the introduction of primarily Ge L_{1c}-derived states lying energetically within the Ge bandgap. We also observe broadening of the energy range within which the Ge L_{1c} character resides. This strong energetic broadening of the CB edge Bloch character is a consequence of C-related alloy disorder. In ordered alloy supercells containing only a single substitutional C impurity, the Born-von Karman boundary conditions generate an ordered alloy in which the C atoms are arranged on a regular grid—determined by

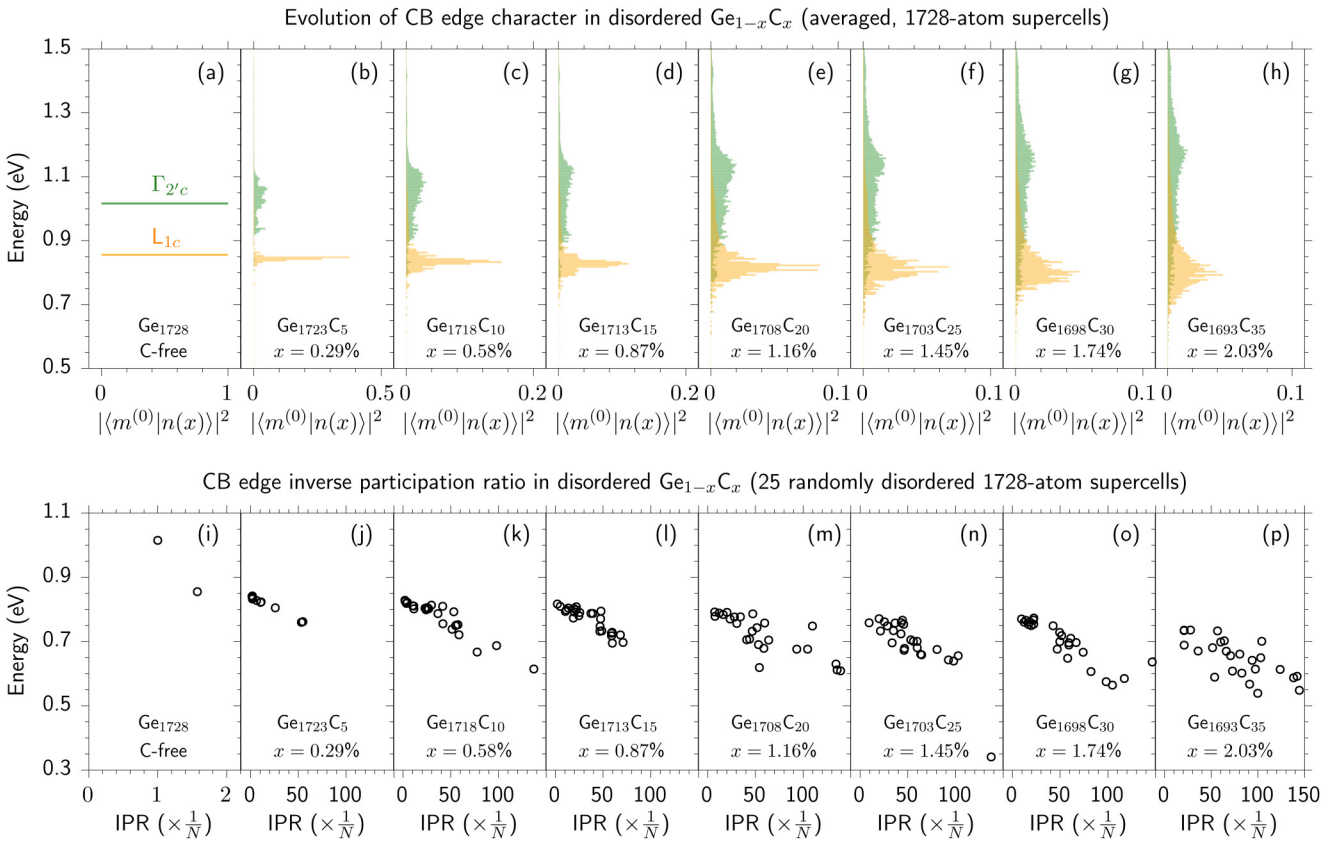

FIG. 4. Top row: Evolution of the character of the alloy CB edge states in 1728-atom disordered $Ge_{1-x}C_x$ supercells. (a) Fractional Ge $\Gamma_{2'c}$ (green) and L_{1c} (orange) character spectra for a C-free Ge_{1728} ($6 \times 6 \times 6$ SC) supercell, calculated, respectively, by projecting the Ge_{1728} CB edge eigenstate $|m^{(0)}\rangle = |\Gamma^{(0)}_{2'c}\rangle$ or $|L^{(0)}_{1c}\rangle$ onto the full set of supercell zone-center ($\mathbf{K} = 0$) eigenstates. (b)–(h), respectively, show the fractional Ge $\Gamma_{2'c}$ and L_{1c} character spectra for a series of disordered, 1728-atom $Ge_{1728-M}C_M$ supercells having $M = 5$–35, in steps of 5 C atoms, corresponding, respectively, to C compositions $x = 0.29\%$, 0.58%, 0.87%, 1.16%, 1.45%, 1.74%, and 2.03%. Note the difference in scales on the abscissae of panels (a), (b), (c)–(d), and (e)–(h). Bottom row: Calculated energy and IPR of the CB edge eigenstate in the 25 distinct, randomly disordered 1728-atom $Ge_{1728-M}C_M$ supercells for which averaged data are presented in the top row. (i) shows the calculated energies and IPRs of the $|\Gamma^{(0)}_{2'c}\rangle$ and $|L^{(0)}_{1c}(A_1)\rangle$ states in C-free Ge_{1728}. (j)–(p), respectively, show the alloy CB edge energies and IPRs calculated for supercells having C compositions $x = 0.29\%$, 0.58%, 0.87%, 1.16%, 1.45%, 1.74%, and 2.03%. Note the difference in scales on the abscissae of panels (i) and (j)–(p).

the supercell lattice vectors—and the underlying cubic symmetry of the diamond lattice is preserved. The calculated Ge character for ordered supercells then resides only on discrete alloy states (cf. Fig. 2), with the associated spectral features having zero width in energy. Substitution of multiple C atoms at randomly selected lattice sites to form a disordered alloy supercell results in short-range structural disorder, breaking the underlying cubic symmetry. This reduction in symmetry, associated with the presence of a wide range of C local neighbor environments, leads in general to the lifting of degeneracies and, in the case of highly-mismatched alloys such as $Ge_{1-x}C_x$, to strong dependence of the calculated electronic properties, including the CB edge energy, on the precise short-range disorder present in a given alloy supercell. The Ge $\Gamma_{2'c}$ and L_{1c} character is then broadened and spread over a continuous energy range in a real $Ge_{1-x}C_x$ alloy, with the degree of energetic broadening reflecting the sensitivity of the electronic structure to short-range structural disorder.

Turning our attention to the averaged Ge $\Gamma_{2'c}$ character in Fig. 4(b), we observe extremely strong energetic broadening. While the Ge L_{1c}-related feature remains sharply defined in energy, we find that alloy disorder gives rise to strong intrinsic inhomogeneous broadening of the Ge $\Gamma_{2'c}$ character. At this C composition $x = 0.29\%$, we find that the maximum Ge $\Gamma_{2'c}$ character residing within a single 5 meV energy interval is 5.4%. We note that this is in contrast to the results shown in Figs. 2(c), 2(h), and 2(m) for small ordered supercells containing a single C atom, where the Ge $\Gamma_{2'c}$ character resides on only a small number of alloy CB levels. Our calculations therefore suggest that C-related alloy disorder leads to strong inhomogeneous energetic broadening of the Ge $\Gamma_{2'c}$ character. Similarly to the ordered supercell calculations of Sec. III A, we find that states lying in the same energy interval generally possess an admixture of both Ge $\Gamma_{2'c}$ and L_{1c} character—i.e., they are hybridized states formed of a linear combination of Ge host matrix states. The $\Gamma_{2'c}$ character is found predominantly at

higher energies, with only a limited amount of $\Gamma_{2'c}$ character mixing into the lowest energy CB states. By comparison, we find that the alloy supercell VB edge states (not shown) retain strong Ge $\Gamma_{25'v}$ character and display comparatively minor energetic broadening, reflecting that C incorporation has minimal impact on the VB structure.

As x is further increased, we note the continuation of this general trend. First, the feature associated with the Ge L_{1c} character is both shifted downward and increasingly broadened in energy with increasing x. Second, we observe extremely strong inhomogeneous broadening of the Ge $\Gamma_{2'c}$ character, which becomes spread over a broad range of energies at and above the CB edge in a given alloy supercell. Thirdly, we note that states lying close in energy to the alloy CB edge acquire minimal Ge $\Gamma_{2'c}$ character and remain primarily Ge L_{1c}-derived. This describes that the fundamental alloy bandgap remains primarily indirect in character, similar to that in Ge, but that spectral features associated with this bandgap undergo strong inhomogeneous broadening due to the presence of alloy disorder. Again, we note that this behavior is markedly different to that expected on the basis of the BAC model, whereby a direct bandgap would be expected to emerge via the transfer of increasing Ge $\Gamma_{2'c}$ character to the alloy CB edge with increasing C composition x. In general, the results of our disordered alloy analysis support the conclusions of Kirwan *et al.*,[27] and of our ordered supercell analysis in Sec. III B above: dilute C incorporation in Ge does not give rise to a direct bandgap. Given the small $\Gamma_{2'c}$ character associated with individual $Ge_{1-x}C_x$ CB states, we do not expect strong optical matrix elements and direct-gap optical recombination between these states and the VB edge.

Finally, the calculated strong inhomogeneous broadening of the Ge $\Gamma_{2'c}$ and L_{1c} character suggests the formation of a distribution of C-related localized states close in energy to the CB edge in $Ge_{1-x}C_x$ alloys. Given that an isolated C impurity generates minimal localization at the CB edge (cf. Sec. III C), this suggests that C-related alloy disorder—i.e., the formation of nearest-neighbor C–C pairs and even near-neighbor C pairs, as well as larger clusters of neighboring C atoms—can generate significant electron localization. To ascertain the extent to which this is the case, at each C composition x we have computed the IPR associated with the lowest energy CB eigenstate in each of the 25 randomly disordered $Ge_{1728-M}C_M$ supercells for which averaged data are presented in Figs. 4(a)–4(h). The calculated energies and IPRs of these states are shown in Figs. 4(i)–4(p). Recalling that a larger IPR reflects stronger localization, we first note a general trend in the calculated IPRs for distinct supercells at fixed x: the IPR associated with a given eigenstate tends to increase strongly with decreasing eigenstate energy. This reflects the emergence of tightly-bound C-related cluster states lying deep within the Ge host matrix bandgap in energy—related predominantly here to the presence of C atoms in close proximity to one another—similar to the distribution of N-related cluster states in dilute nitride $GaN_x(As,P)_{1-x}$.[59,83] Second, we note that the localization of the lowest energy CB state in $Ge_{1-x}C_x$ tends on average to increase with increasing x, reflecting the formation of more localized states in response to the closer proximity of substitutional C atoms at higher C compositions. Thirdly, at fixed x, we note the spread in energy of the lowest energy alloy CB state in distinct randomly disordered supercells, which tends to increase with increasing x and is $\gtrsim 0.2$ eV for the highest C composition considered. This accounts for the strong inhomogeneous broadening of the CB states observed in Figs. 4(a)–4(h) and confirms that the strong sensitivity of the electronic structure to short-range alloy disorder is a consequence of electron localization about clusters of substitutional C atoms. As an extreme example of this localization, we note that the CB edge eigenstate in one of the $Ge_{1703}C_{25}$ ($x = 1.45\%$) supercells considered has both a markedly low energy of 0.341 eV and a high IPR of $\frac{137}{N}$ [visible in the bottom right-hand corner of Fig. 4(n)]. Further inspection reveals that this highly localized CB edge eigenstate is associated with the presence of a C-Ge-C-Ge-C nearest-neighbor chain in the supercell, about which the calculated eigenstate is strongly localized [with its probability density distributed over only $\left(\frac{137}{N}\right)^{-1} \approx 13$ atoms in total].

IV. IMPLICATIONS FOR DEVICE APPLICATIONS

Previous analysis has suggested the emergence of a direct bandgap in dilute $Ge_{1-x}C_x$ alloys and that the resulting alloy band structure should produce performance in $Ge_{1-x}C_x$-based semiconductor lasers and modulators which is comparable to that in conventional direct-gap III-V semiconductor materials.[24] Conversely, the results of our detailed analysis of electronic structure evolution in $Ge_{1-x}C_x$ alloys have negative implications from the perspective of potential device applications.

First, our calculations for ordered alloy supercells suggest that the large differences in size and electronegativity between C and Ge drive hybridization between Ge host matrix states lying close in energy to the CB edge. While this C-induced band mixing results in the transfer of some direct (Ge $\Gamma_{2'c}$) character to the alloy CB edge, this direct-gap character in general remains minimal. Indeed, we confirmed that dilute $Ge_{1-x}C_x$ admits a quasidirect bandgap: while supercell electronic structure calculations show the CB minimum to lie at $\mathbf{K} = 0$, the alloy CB edge, and hence bandgap, retains primarily indirect character.

Second, our analysis of large disordered alloy supercells also demonstrates strong sensitivity of the $Ge_{1-x}C_x$ electronic properties to the presence of short-range alloy disorder, behavior typical of a highly-mismatched semiconductor alloy. In the presence of alloy disorder, our calculations describe a breakdown of the CB edge Bloch character, leading to a broad distribution of C-related localized states lying below the Ge CB edge in energy. Individually, these states possess only minimal direct (Ge $\Gamma_{2'c}$) character and so will not support appreciable direct-gap optical recombination. Further analysis would be required to estimate the magnitude of the optical recombination rate associated with these localized states in a realistic, disordered $Ge_{1-x}C_x$ alloy. Such analysis is beyond the scope of this work, but, based on our calculated $\Gamma_{2'c}$ character spectra (cf. Fig. 4), we would expect a considerably lower radiative recombination rate in dilute $Ge_{1-x}C_x$ than in a conventional direct-gap semiconductor.

From the perspective of carrier transport, experimental measurements for closely-related dilute $Si_{1-x}C_x$ alloys show significant degradation in electron mobility in response to C incorporation. Theoretical analysis by Vaughan *et al.* has demonstrated that the electron mobility in dilute $Si_{1-x}C_x$ is limited not only by C-related alloy scattering, but also by electrically active crystalline defects.

Based on our electronic structure analysis here, we similarly expect a strong C-induced reduction of the electron mobility in dilute $Ge_{1-x}C_x$ alloys. The identification in our disordered supercell calculations of strong inhomogeneous energetic broadening of the CB edge Bloch character reflects the presence of a distribution of localized states and indicates a breakdown of strict **k**-selection. On this basis, we expect many scattering pathways to become available for electrons in the $Ge_{1-x}C_x$ CB, so that the electron mobility in the alloy is both strongly and intrinsically limited.

We emphasize that the conclusions drawn above are based solely on the results of our analysis of the electronic structure of idealized $Ge_{1-x}C_x$ alloys—i.e., purely substitutional, defect-free alloys. The presence of defects—e.g., in the form of C interstitials due to nonsubstitutional incorporation—will likely exacerbate these intrinsic limitations on the optical and transport properties. Overall, while dilute $Ge_{1-x}C_x$ alloys are of interest from a fundamental perspective due to their unusual electronic properties, we conclude that they are likely to be of limited value for applications in CMOS-compatible optoelectronic devices.

V. CONCLUSIONS

In summary, we have presented a theoretical analysis of electronic structure evolution in the group-IV dilute carbide alloy $Ge_{1-x}C_x$. Our calculations were based on a computationally efficient and highly-scalable semiempirical atomistic framework, consisting of (i) structural relaxation using a VFF potential and (ii) electronic structure calculations using a sp^3s^* TB Hamiltonian. Both the VFF potential and the TB Hamiltonian were parameterized based on hybrid functional DFT calculations of the structural, elastic, and electronic properties of the constituent diamond-structured elemental semiconductors Ge and C, as well as the IV-IV compound semiconductor zb-GeC. The validity of this framework has been established by comparison to the results of hybrid functional DFT calculations for small alloy supercells containing up to 128 atoms, where good qualitative and quantitative agreement is found for the nature and evolution of the alloy bandgap. Using this framework, we investigated the evolution with C composition x of the electronic structure of idealized (ordered) and realistic (disordered) $Ge_{1-x}C_x$ alloys.

Recently, it has been suggested that C incorporation in Ge drives the evolution of a direct bandgap via the formation of C-related localized impurity states, with these C-related states undergoing a BAC interaction with the extended Γ_{7c} zone-center CB edge states of the Ge host matrix semiconductor. Contrary to this suggestion, our calculations for ordered $Ge_{1-x}C_x$ alloys revealed the presence of weak C-induced mixing of Ge Γ_{7c} character into the alloy CB edge state. As such, rather than being formed via a BAC interaction of an admixture of a C-related localized impurity state, we showed that the CB edge in ordered $Ge_{1-x}C_x$ alloy supercells is predominantly formed of an A_1-symmetric (s-like) linear combination of the extended L_{6c} CB edge states of Ge. Consequently, we demonstrated that the lowest energy CB state in ordered $Ge_{1-x}C_x$ supercells displays minimal localization about C lattice sites as the ultradilute limit is approached.

For large, disordered $Ge_{1-x}C_x$ alloy supercells, we calculated the evolution of the electronic structure up to $x = 2\%$. Generally, we found that the lowest energy $Ge_{1-x}C_x$ alloy CB states acquire only a minimal admixture of Ge Γ_{7c} (direct-gap) character while retaining predominantly Ge L_{6c} (indirect-gap) character. With increasing x, our calculations revealed that C-related alloy disorder leads to strong inhomogeneous energetic broadening of the Bloch character associated with the CB edge states, due to the formation of a distribution of localized states, associated with C clustering and lying energetically within the Ge bandgap. The formation of a distribution of localized states within the Ge bandgap indicates that dilute $Ge_{1-x}C_x$ alloys are likely to possess intrinsically poor optical and transport properties. On average, we calculated that the direct (Ge Γ_{7c}) character becomes distributed across a multiplicity of higher energy alloy CB states with increasing C composition x, behavior which is markedly different to that expected based on the BAC model.

In conclusion, rather than acquiring a direct bandgap via a BAC interaction, our analysis demonstrates that the $Ge_{1-x}C_x$ CB edge attains minimal direct character. The C-induced band mixing identified by our calculations instead leads to the formation of a quasidirect hybridized alloy bandgap in the dilute C limit, which retains predominantly indirect (Ge L_{6c}) character, with a distribution of C localized states emerging within the Ge bandgap in the presence of short-range alloy disorder. These general conclusions are in qualitative and quantitative agreement with those of recent analysis based on hybrid functional DFT calculations.[27] We therefore conclude that C incorporation in Ge does not give rise to a direct-gap semiconductor alloy, limiting the potential of this material system for applications in optoelectronic devices.

ACKNOWLEDGMENTS

This work was supported by Science Foundation Ireland (SFI; Project No. 15/IA/3082) and by the National University of Ireland (NUI; via the Post-Doctoral Fellowship in the Sciences, held by C.A.B.). The authors thank Ms. Amy C. Kirwan and Dr. Stefan Schulz (Tyndall National Institute, Ireland) for useful discussions and for providing access to the results of their theoretical calculations prior to publication.

REFERENCES

[1]Z. Zhou, B. Yin, and J. Michel, Light Sci. Appl. **4**, e358 (2015).
[2]S. Saito, A. Z. Al-Attili, K. Oda, and Y. Ishikawa, Semicond. Sci. Technol. **31**, 043002 (2016).
[3]D. Thomson, A. Zilkie, J. E. Bowers, T. Komljenovic, G. T. Reed, L. Vivien, D. Marris-Morini, E. Cassan, L. Virot, J.-M. Fédéli *et al.*, J. Opt. **18**, 073003 (2016).
[4]M. Yamaguchi, T. Takamoto, K. Araki, and N. J. Ekins-Daukes, Solar Energy **79**, 78 (2005).
[5]M. Yamaguchi, K.-I. Nishimura, T. Sasaki, H. Suzuki, K. Arafune, N. Kojima, Y. Ohsita, Y. Okada, A. Yamamoto, T. Takamoto *et al.*, Solar Energy **82**, 173 (2008).
[6]R. Roucka, A. Clark, T. Wilson, T. Thomas, M. Führer, N. J. Ekins-Daukes, A. Johnson, R. Hoffman, and D. Begarney, IEEE J. Photovolt. **6**, 1025 (2016).
[7]R. Geiger, T. Zabel, and H. Sigg, Front. Mater. **2**, 52 (2015).
[8]V. Reboud, A. Gassenq, J. M. Hartmann, J. Widiez, L. Virot, J. Aubin, K. Guilloy, S. Tardif, J. M. Fédéli, N. Pauc *et al.*, Prog. Cryst. Growth Charact. **63**, 1 (2017).
[9]F. Zhang, V. H. Crespi, and P. Zhang, Phys. Rev. Lett. **102**, 156401 (2009).
[10]M. E. Kurdia, H. Bertin, E. Martincic, M. de Kersauson, G. Fishman, S. Sauvage, A. Bosseboeuf, and P. Boucauda, Appl. Phys. Lett. **96**, 041909 (2010).

[11]J. R. Sánchez-Pérez, C. Boztug, F. Chen, F. F. Sudradjat, D. M. Paskiewicz, R. B. Jacobson, M. G. Lagally, and R. Paiella, Proc. Natl. Acad. Sci. U.S.A. **108**, 18893 (2011).
[12]M. J. Süess, R. Geiger, R. A. Minamisawa, G. Schiefler, J. Frigerio, D. Chrastina, G. Isella, R. Spolenak, J. Faist, and H. Sigg, Nat. Photonics **7**, 466 (2013).
[13]J. Kouvetakis, J. Menendez, and A. V. G. Chizmeshya, Annu. Rev. Mater. Res. **36**, 497 (2006).
[14]P. Moontragoon, Z. Ikonić, and P. Harrison, Semicond. Sci. Technol. **22**, 742 (2007).
[15]R. Soref, Phil. Trans. R. Soc. A **372**, 0113 (2014).
[16]S. Zaima, O. Nakatsuka, N. Taoka, M. Kurosawa, W. Takeuchi, and M. Sakashita, Sci. Technol. Adv. Mater. **16**, 043502 (2015).
[17]S. Wirths, R. Geiger, N. von den Driesch, G. Mussler, T. Stoica, S. Mantl, Z. Ikonic, M. Luysberg, S. Chiussi, J. M. Hartmann *et al.*, Nat. Photonics **9**, 88 (2015).
[18]J. Margetis, Y. Zhou, W. Dou, P. C. Grant, B. Alharthi *et al.*, Appl. Phys. Lett. **113**, 221104 (2018).
[19]W. Huang, B. Cheng, C. Xue, and C. Li, Physica B **443**, 43 (2014).
[20]W. Huang, B. Cheng, C. Xue, and H. Yang, J. Alloy Compd. **701**, 816 (2017).
[21]H. Alahmad, A. Mosleh, M. Alher, S. Fahimeh Banihashemian, S. A. Ghetmiri, S. Al-Kabi, W. Du, B. Li, S.-Q. Yu *et al.*, J. Electron. Mater. **47**, 3733 (2018).
[22]X. Liu, J. Zheng, L. Zhou, Z. Liu, Y. Zuo, C. Xueab, and B. Cheng, J. Alloy Compd. **785**, 228 (2019).
[23]C. A. Broderick, E. J. O'Halloran, and E. P. O'Reilly, "First principles analysis of electronic structure evolution and the indirect- to direct-gap transition in $Ge_{1-x}Pb_x$ group-IV alloys," e-print arXiv:1911.05679v1 (2019).
[24]C. A. Stephenson, W. A. O'Brien, M. W. Penninger, W. F. Schneider, M. Gillett-Kunnath, J. Zajicek, K. M. Yu, R. Kudraweic, R. A. Stillwell, and M. A. Wistey, J. Appl. Phys. **120**, 053102 (2016).
[25]C. A. Stephenson, W. A. O'Brien, M. Qi, M. W. Penninger, W. F. Schneider, and M. A. Wistey, J. Electron. Mater. **45**, 2121 (2016).
[26]C. A. Broderick, M. D. Dunne, D. S. P. Tanner, A. C. Kirwan, E. J. O'Halloran, S. Schulz, and E. P. O'Reilly, in *Proceedings of the 18th IEEE International Conference on Nanotechnology* (IEEE, 2018).
[27]A. C. Kirwan, S. Schulz, and E. P. O'Reilly, Semicond. Sci. Technol. **34**, 075007 (2019).
[28]H. J. Osten, B. Dietrich, H. Rücker, and M. Methfessel, J. Cryst. Growth **150**, 931 (1995).
[29]S. C. Jain, H. J. Osten, B. Dietrich, and H. Rücker, Semicond. Sci. Technol. **10**, 1289 (1995).
[30]E. Finkman, F. Meyer, and M. Mamor, J. Appl. Phys. **89**, 2580 (2001).
[31]H. Rücker, M. Methfessel, B. Dietrich, K. Pressel, and H. J. Osten, Phys. Rev. B **53**, 1302 (1996).
[32]M. P. Vaughan, F. Murphy-Armando, and S. Fahy, Phys. Rev. B **85**, 165209 (2012).
[33]M. Okinaka, K. Miyatake, J. Ohta, and M. Nunoshita, J. Cryst. Growth **255**, 273 (2003).
[34]K. J. Roe, M. W. Dashiell, J. Kolodzey, P. Bouchaud, and J.-M. Lourtioz, J. Vac. Sci. Technol. B **17**, 1301 (1999).
[35]J. Kolodzey, P. R. Berger, B. A. Orner, D. Hits, F. Chen, A. Khan, X. Shao, M. M. Waite, S. I. Shah, C. P. Swann *et al.*, J. Cryst. Growth **157**, 386 (1995).
[36]D. Gall, J. D'Arcy-Gall, and J. E. Greene, Phys. Rev. B **62**, R7723(R) (2000).
[37]S. Y. Park, J. D'Arcy-Gall, D. Gall, Y.-W. Kim, P. Desjardins, and J. E. Greene, J. Appl. Phys. **91**, 3644 (2002).
[38]C. A. Stephenson, M. Gillett-Kunnath, W. A. O'Brien, R. Kudraweic, and M. A. Wistey, Crystals **6**, 159 (2016).
[39]W. Shan, W. Walukiewicz, J. W. A. III, E. E. Haller, J. F. Geisz, D. J. Friedman, J. M. Olson, and S. R. Kurtz, Phys. Rev. Lett. **82**, 1221 (1999).
[40]J. Wu, W. Shan, and W. Walukiewicz, Semicond. Sci. Technol. **17**, 860 (2002).
[41]J. Wu, W. Walukiewicz, K. M. Yu, J. W. A. III, E. E. Haller, I. Miotkowski, A. K. Ramdas, C.-H. Su, I. K. Sou, R. C. C. Perera *et al.*, Phys. Rev. B **67**, 035207 (2003).
[42]E. P. O'Reilly, A. Lindsay, P. J. Klar, A. Polimeni, and M. Capizzi, Semicond. Sci. Technol. **24**, 033001 (2009).
[43]D. S. P. Tanner, Ph.D. thesis (University College Cork, Ireland, 2017), see http://cora.ucc.ie/handle/10468/5459.
[44]D. S. P. Tanner, C. A. Broderick, A. C. Kirwan, S. Schulz, and E. P. O'Reilly, "Elastic properties of elemental, compound, and alloyed group-IV materials: Hybrid density functional theory and valence force field parametrisation" (unpublished).
[45]C. A. Broderick, A. C. Kirwan, S. Schulz, and E. P. O'Reilly, "Electronic properties of elemental and compound group-IV materials: Hybrid density functional theory and tight-binding parametrisation" (unpublished).
[46]R. M. Martin, Phys. Rev. B **1**, 4005 (1970).
[47]M. J. P. Musgrave and J. A. Pople, Proc. R. Soc. Lond. A **268**, 474 (1962).
[48]D. S. P. Tanner, M. A. Caro, S. Schulz, and E. P. O'Reilly, "Fully analytic valence force field model for the elastic and inner elastic properties of diamond and zincblende crystals," e-print arXiv:1908.11245 (2019).
[49]J. D. Gale, JCS Faraday Trans. **93**, 629 (1997).
[50]J. D. Gale and A. L. Rohl, Mol. Simul. **29**, 291 (2003).
[51]J. D. Gale, Z. Krist. **220**, 552 (2005).
[52]E. P. O'Reilly and A. Lindsay, J. Phys. Conf. Ser. **242**, 012002 (2010).
[53]P. Vogl, H. P. Hjalmarson, and J. D. Dow, J. Phys. Chem. Solids **44**, 365 (1983).
[54]E. J. O'Halloran, C. A. Broderick, D. S. P. Tanner, S. Schulz, and E. P. O'Reilly, Opt. Quant. Electron. **51**, 314 (2019).
[55]M. S. Dresselhaus, G. Dresselhaus, and A. Jorio, *Group Theory: Application to the Physics of Condensed Matter* (Springer, 2008).
[56]J.-M. Jancu, R. Scholz, F. Beltram, and F. Bassani, Phys. Rev. B **57**, 6493 (1998).
[57]A. Lindsay and E. P. O'Reilly, Solid State Commun. **112**, 443 (1999).
[58]E. P. O'Reilly, A. Lindsay, S. Tomić, and M. Kamal-Saadi, Semicond. Sci. Technol. **17**, 870 (2002).
[59]A. Lindsay and E. P. O'Reilly, Phys. Rev. Lett. **93**, 196402 (2004).
[60]A. Lindsay and E. P. O'Reilly, Phys. Rev. B **76**, 075210 (2007).
[61]A. Lindsay and E. P. O'Reilly, Phys. Status Solidi C **5**, 454 (2008).
[62]T. Sander, J. Teubert, P. J. Klar, A. Lindsay, and E. P. O'Reilly, Phys. Rev. B **83**, 235213 (2011).
[63]M. Usman, C. A. Broderick, A. Lindsay, and E. P. O'Reilly, Phys. Rev. B **84**, 245202 (2011).
[64]M. Usman, C. A. Broderick, Z. Batool, K. Hild, T. J. C. Hosea, S. J. Sweeney, and E. P. O'Reilly, Phys. Rev. B **87**, 115104 (2013).
[65]C. A. Broderick, S. Mazzucato, H. Carrère, T. Amand, H. Makhloufi, A. Arnoult, C. Fontaine, O. Donmez, A. Erol, M. Usman *et al.*, Phys. Rev. B **90**, 195301 (2014).
[66]M. Usman, C. A. Broderick, and E. P. O'Reilly, Phys. Rev. Appl. **10**, 044024 (2018).
[67]L. Brey, C. Tejedor, and J. A. Vergés, Phys. Rev. B **29**, 6840 (1984).
[68]C. Priester, G. Allan, and M. Lannoo, Phys. Rev. B **37**, 8519(R) (1988).
[69]J. C. Slater and G. F. Koster, Phys. Rev. **94**, 1498 (1954).
[70]H. Rücker, R. Enderlein, and F. Bechstedt, Phys. Status Solidi B **153**, 595 (1989).
[71]M. C. Muñoz and G. Armelles, Phys. Rev. B **48**, 2839 (1993).
[72]Y.-H. Li, A. Walsh, S. Chen, W.-J. Yin, J.-H. Yang, J. Li, J. L. F. D. Silva, X. G. Gong, and S.-H. Wei, Appl. Phys. Lett. **94**, 212109 (2009).
[73]A. C. Kirwan, E. J. O'Halloran, C. A. Broderick, S. Schulz, and E. P. O'Reilly, in *Proceedings of the 18th IEEE International Conference on Nanotechnology* (IEEE, 2018).

[74]T. D. Eales, I. P. Marko, S. Schulz, E. J. O'Halloran, S. Ghetmiri, W. Du, Y. Zhou, S.-Q. Yu, J. Margetis, J. Tolle *et al.*, Sci. Rep. **9**, 14077 (2019).
[75]D. J. Thouless, Phys. Rep. **13**, 93 (1974).
[76]D. S. P. Tanner, M. A. Caro, E. P. O'Reilly, and S. Schulz, RSC Adv. **6**, 64513 (2016).
[77]A. Lindsay and E. P. O'Reilly, Physica E **21**, 901 (2004).
[78]C. Harris, A. Lindsay, and E. P. O'Reilly, J. Phys. Condens. Matter **20**, 295211 (2008).
[79]Y. Zhang and L.-W. Wang, Phys. Rev. B **83**, 165208 (2011).
[80]P. R. C. Kent, L. Bellaiche, and A. Zunger, Semicond. Sci. Technol. **17**, 851 (2002).
[81]C. A. Broderick, M. Seifikar, E. P. O'Reilly, and J. M. Rorison, *Dilute Nitride Alloys, Handbook of Optoelectronic Device Modeling and Simulation* (CRC Press, 2017), Vol. 1, Chap. 9.
[82]C. A. Broderick, I. P. Marko, E. P. O'Reilly, and S. J. Sweeney, *Dilute Bismide Alloys, Handbook of Optoelectronic Device Modeling and Simulation* (CRC Press, 2017), Vol. 1, Chap. 10.
[83]P. R. C. Kent and A. Zunger, Phys. Rev. B **64**, 115208 (2001).